CHEMISTRY
A EUROPEAN JOURNAL

DOI: 10.1002/chem.201001452

VIP

New Insight into the Conventional Replacement Reaction for the Large-Scale Synthesis of Various Metal Nanostructures and their Formation Mechanism

Gaixia Zhang, Shuhui Sun, Ruying Li, and Xueliang Sun*[a]

Metal nanomaterials have attracted considerable interest, because of their unique size- and shape-dependent chemical and physical properties,[1] as well as their potential applications in catalysis,[2,3] information storage,[4] electrochemical devices,[5] and biological and chemical sensing.[6,7] Most methods reported so far for synthesizing such materials have focused on template or surfactant processes,[8,9] electrochemical depositions[10,11] and sol–gel approaches.[12] However, such methods require that either the template/surfactant/substrate be thoroughly removed for purifying the product or the reaction be conducted at elevated temperatures. Thus, there still remains much interest in exploring simpler and more versatile synthetic routes with a more wise control of nanomaterial morphology and structure.

Galvanic replacement (transmetalation) reactions have a long history. However, it is only recently that approaches for synthesizing nanomaterials based on this reaction, involving sacrificial metals and suitable metal ions, have been employed and developed. Xia et al.[13–16] and Sastry et al.[17,18] synthesized Pt, Au, and AuPt hollow structures by using pre-synthesized Ag nanostructures as templates by means of replacement reactions. Bai et al. synthesized Pt and AuPt bimetallic hollow nanostructures,[19–21] exploiting pre-synthesized Co nanoparticles as sacrificial templates. Ag and Co are expensive metals, and the pre-synthesizing processes of these nanostructure templates further increase the cost; in addition, AgCl precipitated in the solution during reaction, which complicated the procedure and also influenced the yield of hollow products. Bhargava et al.[22] used a galvanic replacement reaction to create Cu nanoscale pores in Ni foil. By employing the galvanic reaction between aqueous $[Ag(NH_3)_2]OH$ and a copper plate, Yao et al.[23] obtained a superhydrophobic pure silver film with flower-like microstructures. These porous structures were synthesized on bulk foil substrates, which may limit their applications.

Here, we report a simple, cost effective and versatile strategy, which we call the commercial sacrificial metal-based replacement reaction (CSMRR), for synthesizing various metals (including magnetic, rare-earth, noble, etc.) with a series of novel nanostructures. The key difference between our method and those reported previously is that this is the first time very cheap, commercially available Mg/Al powders have been used, rather than any pre-synthesized nanostructures or bulk materials, to reduce the desired metal salt precursors. Specifically, the use of such Mg/Al powders as sacrificial metals has the following main advantages:

1) Their redox pair potentials are very low [Mg^{2+}/Mg (−2.356 V) and Al^{3+}/Al (−1.676 V) vs. the standard hydrogen electrode (SHE)][24] and they are very reactive, so that most metals (as long as their redox potentials are higher than that of Mg^{2+}/Mg or Al^{3+}/Al) could be reduced from their corresponding salt solutions.
2) The reactions can be conducted very efficiently, even at room temperature.
3) The products can be purified and collected easily compared with those obtained involving a surfactant or template.
4) The amount of product can easily be scaled up by simply multiplying the amounts of reactants, which enables mass production.
5) They are commercially available and much cheaper than commonly used Ag, Pd, Cu, Co, and Ni bulk metals (let alone their pre-synthesized nanostructures).
6) By using Mg or Al, the as-synthesized metal structures are related to the difference in the metal potentials (net potentials), as well as to the composition and the concentration of the metal salt precursors rather than to the structures of the sacrificial metal templates. This makes nanostructure synthesis more adjustable and reproducible.

[a] Dr. G. Zhang, Dr. S. Sun, R. Li, Prof. X. Sun
Department of Mechanical and Materials Engineering
The University of Western Ontario, London
Ontario, N6A 5B9 (Canada)
Fax: (+1) 519-661-3020
E-mail: xsun@eng.uwo.ca

Supporting information for this article is available on the WWW under http://dx.doi.org/10.1002/chem.201001452.

In addition, our work also reveals the importance of the simplicity in scientific research; the simplest, natural method, often overlooked, may indeed yield exciting results.

To reveal the capability of this strategy, using Ni as the sample metal, we have shown in detail that this approach can produce various structures such as 1D nanowires that are $\approx$15 nm in diameter, 2D nanoribbons that are a few nanometers thick, and self-assembled 3D flowers that have a porous structure. This systematic control of the dimensions and shapes of Ni structures, to the best of our knowledge, has never been reported before.[25–28]

The Ni nanowires were synthesized by the replacement reaction between commercial Mg powder and $NiCl_2$ in aqueous solution, based on the reaction given in Equation (1).

$$Mg_{(s)} + Ni^{2+}{}_{(aq)} \rightarrow Ni_{(s)} + Mg^{2+}{}_{(aq)} \quad (1)$$

Significantly, the amount of product can be easily scaled up to kilogram scale (e.g., 0.45 kg, inset of Figure 1) in one pot by simply multiplying the amounts of reactants (see Supporting Information Figure S1 A–C). The powder X-ray diffraction (XRD) pattern of the Ni product (Figure 1 A) matches well with the Ni face-centered cubic (fcc) structure (JCPCDS, 04-0850), indicating its good crystallinity. The scanning electron microscopy (SEM) and transmission electron microscopy (TEM) images (Figure 1 B and Figure S1 D,E in the Supporting Information) show that numerous uniform wirelike structures, tens of micrometers long with mean diameter of 15.4 ± 7.2 nm (Figure S1 F in the Supporting Information), are obtained. Under higher magnification TEM investigation (Figure 1 C), evident tubelike nanostructures with asymmetric mass contrasts, as well as the appearance of the sheetlike structures at the edges, are seen, which indicate the Ni nanowires actually are scroll-like structures. The energy-dispersive X-ray spectrum (EDX, Figure S1 G in the Supporting Information) demonstrates the purity of Ni product. For a complete view of the scroll formation process, a growth and morphological evolution study was conducted as a function of reaction time, and the products were examined by TEM. As shown clearly in Figure S2 in the Supporting Information, on sacrificing Mg atoms the Ni atoms first precipitate and form tiny sheetlike structures on the surface of Mg particles (Figure S2 A,A′ and B,B′ in the Supporting Information); with time, the nanosheets grow longer and wider, and start to roll up (Figure S2 C,C′ and D,D′ in the Supporting Information), and, finally, they form complete nanoscrolls (Figure S2 E,E′ in the Supporting Information). A high-resolution TEM (HRTEM) image (Figure 1 D, white square in Figure 1 C) with visible lattice fringes, and the corresponding fast Fourier transformation (FFT) (inset), further confirm that the Ni nanostructures are single crystalline. The fringes perpendicular to the nanowire axis are evenly separated by $\approx$0.143 nm, matching the (211) planes of the fcc crystalline Ni. The fringes parallel to the nanowire axis, which have a $\approx$0.248 nm interplanar separation, correspond to the (110) planes; that is, the scroll-like nanowires originate from 2D nanosheets that possess a large difference in interplanar distances in two perpendicular directions. Therefore, whenever there is a structural stress, their unique structure will promote a rolling along the axis parallel to the plans that have the larger interplanar separation, to release the stress.[29]

When we simply substituted the $NiCl_2$ solution with $Ni(NO_3)_2$, in addition to the reaction rate becoming a little slower, both the morphology and structure of the Ni product changed. Figure 2 A and Figure S3 A in the Supporting Information show a cotton-puff-like structure, which is composed of numerous nanoribbons. The EDX spectrum (Fig-

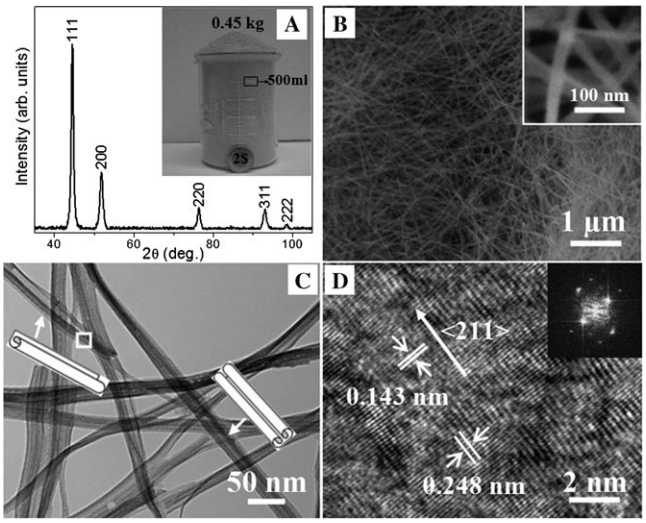

Figure 1. Ni wire-like structures synthesized from Mg and $NiCl_2$. A) XRD pattern, B) SEM image, and C), D) TEM images. The inset in A) is an example of the bulk quantity of Ni nanowire product; the image consists of approximately 0.45 kg of sample, and a Canadian two-dollar coin for comparison.

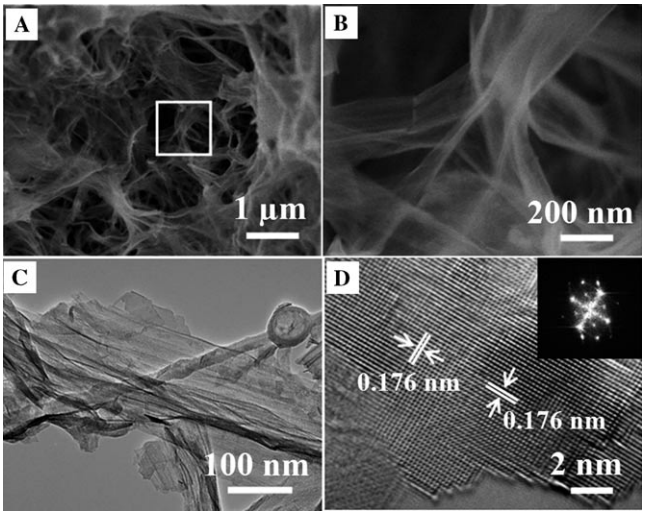

Figure 2. Ni nanoribbons synthesized from Mg and $Ni(NO_3)_2$. A), B) SEM images, and C), D) TEM images of Ni nanoribbons.

ure S3B in the Supporting Information) reveals their purity. These nanoribbons (Figure 2B and C) are a few nanometers thick, several hundreds of nanometers wide, several micrometers long and are smooth, flat, and almost transparent, although they sometimes randomly bend, overlap, or partially roll up (Figure S3C and D in the Supporting Information). The well-ordered and smooth lattice fringes (HRTEM, Figure 2D) as well as the sharp spots in the corresponding FFT (inset, Figure 2D) indicate the crystallinity of the nanoribbons. Clearly visible fringes extend in two directions, with the same lattice spacing of 0.176 nm, revealing that the two growth directions (width and length) are both along ⟨100⟩ orientation. Thus, no preferring rolling direction exists in the original sheets of the nanoribbons, which results in random bending, overlapping, or partial rolling up of the structure, to release the stress whenever it occurs. To further confirm this, we also investigated the formation process of Ni ribbons. As shown in Figure S4 in the Supporting Information, at the beginning, tiny Ni sheetlike structures are formed on the surface of Mg particles (Figure S4A,A′ in the Supporting Information), which is similar to the initial formation stage of Ni nanoscroll (Figure S2A,A′ and B,B′ in the Supporting Information); however, with time, no rolling process happens, but the nanosheet grows wider and longer, with random bending and overlapping (Figure S4B–D and B′–D′ in the Supporting Information). Comparing the Ni scroll- and ribbonlike structures synthesized under the same conditions but with different metal salts, $NiCl_2$ and $Ni(NO_3)_2$, we can see the effect of the anions on nanostructure formation. The exact mechanisms of anion effect are still under investigation. However, as mentioned above, the $Ni(NO_3)_2$ reaction is slower than the $NiCl_2$ reaction, because the existing anions appear to affect the standard reduction potentials (SRP) of the metals to be reduced, which then affects the reaction rate, the growth speeds of different crystal faces, and then the final morphology. In addition, the electronic structures and the polar properties of the anions may also affect the aggregation path of the synthesized metal atoms and, therefore, the final morphology of the metal structure.[30]

We further studied the effect of sacrificial metal on the morphology of the product. When Al was used instead of Mg as the sacrificial metal, with $NiCl_2$ as the precursor, flower-like Ni structures were obtained. The SEM images at different magnifications (Figure 3A and B) reveal that the entire Ni flower structure, with mean diameter of 1.5 ± 0.1 μm (Figure S5B in the Supporting Information), is constructed of several dozen nanosheets that are ≈10 nm thick and a few hundred nanometers wide, connecting to form 3D flower-like structures. In addition, many of the nanosheets bend at their edges, giving the impression of real nanopetals. The purity of the Ni flowers was demonstrated by the EDX spectrum (Figure S5C in the Supporting Information). A representative TEM image (Figure 3C) confirms that the flower structure is formed from uniform petal-like nanosheets and no solid core was observed, which is consistent with the SEM results. The selected area electron diffraction

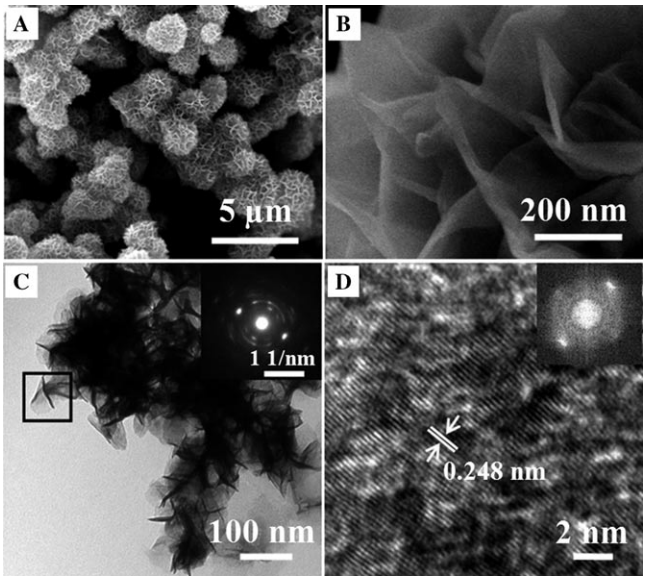

Figure 3. Ni flowers synthesized from Al and $NiCl_2$. A), B) SEM images, and C), D) TEM images of Ni flowers.

(SAED) pattern (inset of Figure 3C) that was taken from several Ni nanopetals (squared in Figure 3C) indicates the crystallinity of the structures. This was also confirmed by the HRTEM image with the corresponding FFT (Figure 3D and inset) obtained from one petal of the Ni flower. The 0.248 nm lattice spacing matches the interplanar separation of the (110) planes of fcc Ni. In addition, a morphological evolution study was conducted as a function of reaction time (Figure S6). Evidently, similar sheetlike structures are formed, but under lower reaction rate, it finally results in flowerlike structure. Comparing the Ni scroll- and flowerlike structures synthesized under the same conditions, but with different sacrificial metals (Mg and Al), we see the effect of the redox potentials on the formation of the nanostructures. That is, the net redox potential of 1.419 V between Ni^{2+}/Ni (−0.257 V) and Al^{3+}/Al (−1.676 V) is much smaller than 2.099 V which is the net potential between Ni^{2+}/Ni (−0.257 V) and Mg^{2+}/Mg (−2.356 V); thus, the replacement reaction of the former (Figure S6 in the Supporting Information) is slower than that of the latter (Figure S2 in the Supporting Information). Therefore, with a lower reaction rate, the Ni atoms reduced by Al will have more time to aggregate and form a thicker nanosheet than those synthesized with Mg.

We also exploited the replacement reaction between Al and $Ni(NO_3)_2$, which produced flowerlike/nanowall-like structures (Figure S7 in the Supporting Information) that were similar to those obtained with Al and $NiCl_2$, but composed of a number of bigger nanosheets with a greater average thickness. This reinforces our hypothesis that there is an anion effect influencing the different morphologies as mentioned above, in our discussion when Mg and $NiCl_2$/$Ni(NO_3)_2$ were used.

In addition, various other metals including transition metals and rare earth group, can be effectively synthesized by this facile CSMRR method. By using commercial Mg as the sacrificial metal and chloride compounds of the desired metals as the precursors only, we sampled two representative metals from each group (Ni and Fe for magnetic, Pd and Pt for noble, V and Mn for other transition metals, as well as La and Ce for rare-earth metals) to demonstrate the power of this approach (Figure 4 and also see the Supporting Information for details, Figures S8–S11). The purities of the products were confirmed by EDX spectra and the detailed size distributions of the metal nanostructures are also provided (Figure S8–S11 in the Supporting Information).

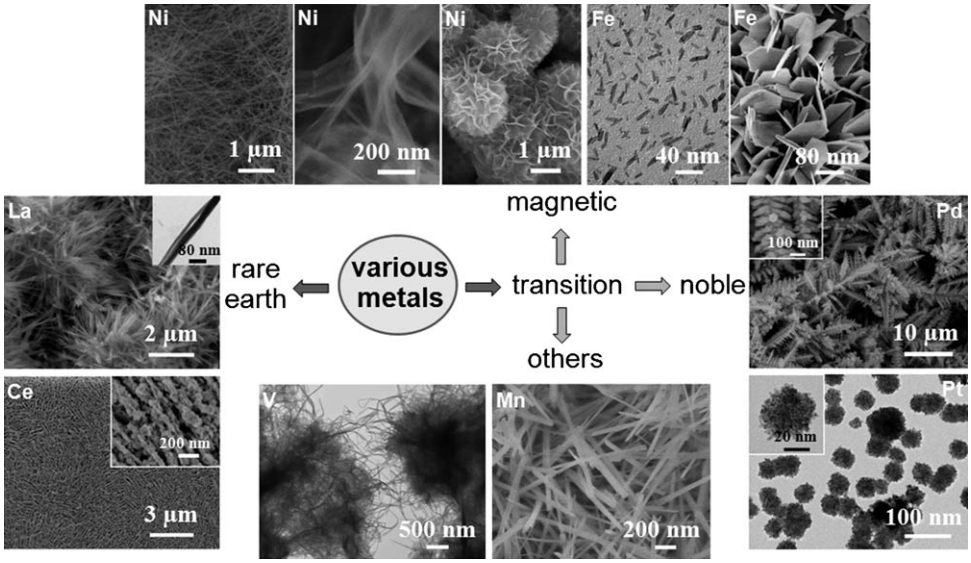

Figure 4. Novel structures of various metals in different groups obtained using CSMRR method. Magnetic metals: Ni nanowires, nanoribbons and nanoflowers; and Fe tiny nanorods and smooth nanosheets synthesized from $FeCl_3$ and $FeCl_2$, respectively. Noble metals: fern-like dendritic Pd structure and self-assembled porous Pt nanospheres synthesized from K_2PdCl_4 and H_2PtCl_6, respectively. Other transition metals: V nanoribbons and Mn nanowires synthesized from VCl_3 and $MnCl_2$, respectively. Rare-earth metals: La nanoscrolls and Ce nanobricks synthesized from $LaCl_3$ and $CeCl_3$, respectively.

From all the above, we believe there are several factors playing key roles in the morphological and structural control of the metals formed via this CSMRR method. The first factor relates to the net redox potential between the redox pairs of the sacrificial metal and the target metal to be synthesized. If different sacrificial metals (e.g., Mg or Al) are used to reduce the same metal salts under the same conditions, different metal structures are obtained (Figures 1 and 3). We call this the Sacrificial Metal Potential Effect (SMPE). However, if the same sacrificial metals and same anions are used, but with different cations (Figures 1 and 4), or with the same cations but different valent states (e.g., Fe^{2+} and Fe^{3+}, Figure 4), different structures are generated. We call this the cation potential effect (CPE). Another important factor is the anion effect (AE, Figures 1 and 2), which arises from the influence of the existing anions in solution on the SRPs of the metals and from the differences in anion electronic structures and polar properties as well. In short, we found that the net redox potential, resulted from two main influences—either from the use of different sacrificial metals and/or different cations (or the same cations with different valent states), and the anion effect are the main factors. Although we have demonstrated that there are other factors such as metal salt concentration or temperature that can alter the structure of the synthesized metals, these will not be discussed here.

In summary, based on the galvanic replacement reaction, we have developed a general, facile strategy (CSMRR) by using commercially available, cost-effective metal (e.g. Mg and Al) powders, rather than any pre-synthesized, expensive metal nanostructures as sacrificial templates, for the mass synthesis of transition and rare-earth metals that have various novel nanostructures, such as wires, ribbons, flowers, rods, sheets, scrolls, spheres, dendrites, and so on. Through a series of time-dependent morphological evolution studies, the growth processes of various Ni nanostructures have been systematically investigated, and several key factors in the morphological and structural control of the metal structures also have been proposed and discussed. In addition, due to their adjustable morphologies, high surface area and unique properties, such novel nanostructures hold great potential in fuel cell, hydrogen storage, pollutant purification, and biological and chemical sensing applications.

Experimental Section

Materials: Nickel(II) chloride hexahydrate ($NiCl_2{\cdot}6H_2O$), nickel(II) nitrate hexahydrate [$Ni(NO_3)_2{\cdot}6H_2O$], iron(III) chloride ($FeCl_3$), iron(II) chloride ($FeCl_2$), potassium tetrachloropalladate(II) (K_2PdCl_4), chloroplatinic acid hexahydrate ($H_2PtCl_6{\cdot}6H_2O$), vanadium(III) chloride (VCl_3), manganese(II) chloride ($MnCl_2$), lanthanum(III) chloride hydrate ($LaCl_3{\cdot}xH_2O$), cerium(III) chloride ($CeCl_3$), and gold(III) chloride trihydrate ($HAuCl_4{\cdot}3H_2O$), were purchased from Sigma–Aldrich and used as received. The metal powders, aluminum (Al, nanopowder) and magnesium (Mg, −100+200 mesh) were obtained from Aldrich and Alfa Aesar, respectively. In the synthesis of the nanostructures, doubly distilled deionized (DI) water was used for all preparations.

Nanostructure synthesis: In a typical synthesis, a controlled amount of freshly prepared metal salt aqueous solution was quickly added to a glass vial that contained a predetermined amount of commercially available sacrificial metal powder (e.g., Mg). To synthesize Ni nanowires, for example, the replacement reaction between Mg (60 mg) and $NiCl_2$ solution (0.5 M, 6 mL) was used, in which the atomic concentration of Ni^{2+} was greater than that of Mg so that the Mg could be completely oxidized to

Mg^{2+}, precipitating Ni nanowires only. The reactions were conducted at room temperature in ambient atmosphere for up to several days. After the reduction reactions were complete, the products were washed several times in DI water, collected by filtration and then dried in an oven at about 40 °C under Ar atmosphere.

Nanostructure characterization: The morphology, crystallinity, and chemical composition of the as-synthesized nanostructures were characterized and analyzed by powder X-ray diffraction (XRD, a Bruker D8 Discover diffractometer, operating at 40 kV and 40 mA) with Cu Kα radiation ($\lambda =$ 0.154 nm), filed-emission scanning electron microscope (FESEM, Hitachi S-4800, operating at 5 kV) equipped with an energy-dispersive X-ray spectrometry (EDX), transmission electron microscope (TEM, Philips CM10 microscope, operating at 100 kV), and high-resolution TEM (HRTEM, JEOL 2010F, operating at 200 kV).

Acknowledgements

This work was supported by NSERC, GM of Canada, CRC Program, CFI, ORF, ERA and UWO. G.Z. is grateful to the Ontario PDF Program. S.S. thanks the NSERC scholarship. We are indebted to Prof. E. Sacher, H. Liu, N. Cason, D. Tweddell, F. Pearson, and Dr. M. Cai for their kind help and fruitful discussions.

Keywords: growth factors · nanostructures · nickel · transmetalation

[1] J. Y. Chen, B. J. Wiley, Y. N. Xia, *Langmuir* **2007**, *23*, 4120–4129.
[2] S. H. Sun, F. Jaouen, J. P. Dodelet, *Adv. Mater.* **2008**, *20*, 3900–3904.
[3] Y. G. Guo, J. S. Hu, L. J. Wan, *Adv. Mater.* **2008**, *20*, 2878–2887.
[4] Y. F. Xu, M. L. Yan, D. J. Sellmver, *J. Nanosci. Nanotechnol.* **2007**, *7*, 206–224.
[5] S. W. Chen, Y. Y. Yang, *J. Am. Chem. Soc.* **2002**, *124*, 5280–5281.
[6] N. Krasteva, I. Besnard, B. Guse, R. E. Bauer, K. Mullen, A. Yasuda, T. Vossmeyer, *Nano Lett.* **2002**, *2*, 551–555.
[7] T. A. Taton, C. A. Mirkin, R. L. Letsinger, *Science* **2000**, *289*, 1757–1760.
[8] C. L. Cheng, J. S. Lin, Y. F. Chen, *Mater. Lett.* **2008**, *62*, 1666–1669.
[9] J. Q. Liu, A. I. Maaroof, L. Wieczorek, M. B. Cortie, *Adv. Mater.* **2005**, *17*, 1276–1281.
[10] B. M. Quinn, C. Dekker, S. G. Lemay, *J. Am. Chem. Soc.* **2005**, *127*, 6146–6147.
[11] Y. Hou, H. Kondoh, T. Ohta, S. Gao, *Appl. Surf. Sci.* **2005**, *241*, 218–222.
[12] F. L. Jia, L. Z. Zhang, X. Y. Shang, Y. Yang, *Adv. Mater.* **2008**, *20*, 1050–1054.
[13] Y. G. Sun, B. T. Mayers, Y. N. Xia, *Nano Lett.* **2002**, *2*, 481–485.
[14] Y. G. Sun, Y. N. Xia, *Adv. Mater.* **2003**, *15*, 695–699.
[15] Y. G. Sun, Y. N. Xia, *J. Am. Chem. Soc.* **2003**, *125*, 3892–3901.
[16] X. M. Lu, H. Y. Tuan, J. Y. Chen, Z. Y. Li, B. A. Korgel, Y. N. Xia, *J. Am. Chem. Soc.* **2007**, *129*, 1733–1742.
[17] P. R. Selvakannan, M. Sastry, *Chem. Commun.* **2005**, 1684–1686.
[18] S. Shukla, A. Priscilla, M. Banerjee, R. R. Bhonde, J. Ghatak, P. V. Satyam, M. Sastry, *Chem. Mater.* **2005**, *17*, 5000–5005.
[19] H. P. Liang, H. M. Zhang, J. S. Hu, Y. G. Guo, L. J. Wan, C. L. Bai, *Angew. Chem.* **2004**, *116*, 1566–1569; *Angew. Chem. Int. Ed.* **2004**, *43*, 1540–1543.
[20] H. P. Liang, L. J. Wan, C. L. Bai, L. Jiang, *J. Phys. Chem. B* **2005**, *109*, 7759–7800.
[21] H. P. Liang, Y. G. Guo, H. M. Zhang, J. S. Hu, L. J. Wan, C. L. Bai, *Chem. Commun.* **2004**, 1496–1497.
[22] V. Bansal, H. Jani, J. D. Plessis, P. J. Coloe, S. K. Bhargava, *Adv. Mater.* **2008**, *20*, 717–723.
[23] Z. W. Cao, D. B. Xiao, L. T. Kang, Z. L. Wang, S. X. Zhang, Y. Ma, H. B. Fu, J. N. Yao, *Chem. Commun.* **2008**, 2692–2694.
[24] C. G. Zoski, *Handbook of Electrochemistry*, Elsevier, Oxford, **2007**, pp. 815–817.
[25] H. Winnischofer, T. C. Rocha, W. C. Nunes, L. M. Socolovsky, M. Knobel, D. Zanchet, *ACS Nano* **2008**, *2*, 1313–1319.
[26] C. M. Liu, L. Guo, R. M. Wang, Y. Deng, H. B. Xu, S. H. Yang, *Chem. Commun.* **2004**, 2726–2727.
[27] H. J. Zheng, J. H. Zhong, Gu, Z. H. W. Wang, *J. Magn. Magn. Mater.* **2008**, *320*, 565–570.
[28] T. Hang, Q. Fei, *Nanotechnology* **2008**, *19*, 035201.
[29] W. Zhang, X. Wen, S. Yang, Y. Berta, Z. Wang, *Adv. Mater.* **2003**, *15*, 822–825.
[30] G. B. Saupe, C. C. Waraksa, H. Kim, Y. J. Han, D. M. Kaschak, D. M. Skinner, T. E. Mallouk, *Chem. Mater.* **2000**, *12*, 1556–1562.

Received: May 25, 2010
Published online: July 28, 2010

